BMC Microbiology

RESEARCH

Open Access

Involvement of *Mycobacterium smegmatis* small noncoding RNA B11 in triacylglycerol accumulation and altered cell wall permeability

Zhuhua Wu[1†], Weilong Liu[3†], Qiuchan Tan[4], Yuhui Chen[1], Xiaoyu Lai[1], Jianming Hong[2], Hongdi Liang[1], Huizhong Wu[1*], Jing Liang[2*] and Xunxun Chen[1*]

Abstract

Background Pathways involving triacylglycerol (TAG) accumulation are thought to play a crucial regulatory role in bacterial growth and metabolism. Despite this understanding, little is known about the biological functions and regulatory mechanisms of small RNAs in *Mycobacterium*. *Mycobacterium smegmatis* (*M. smegmatis*), a type of *Mycobacterium*, serves as a model organism to investigate the molecular, physiological, and drug resistance features of *M. tuberculosis*.

Results In this study, we demonstrated that overexpression of B11 significantly affects bacterial growth and colony morphology, increases antibiotic sensitivity and sodium dodecyl sulfate (SDS) surface stress, decreases intracellular survival, and suppresses cytokine secretion in macrophages. Transcriptomic and lipidomic analyses revealed a metabolic downshift in the B11 overexpression strain, characterized by reduced levels of TAG. Furthermore, transmission electron microscopy showed that the B11 overexpression strain exhibited decreased cell wall thickness, leading to reduced biofilm formation and altered cell wall permeability. Additionally, we observed that B11 regulated certain target genes but did not directly bind to those proteins tested.

Conclusions Taken together, these findings suggest that B11 plays important roles in *Mycobacterium* survival under antibiotic and SDS stresses, TAG accumulation, and contributes to antibiotic sensitivity through altered cell wall permeability.

Keywords *Mycobacterium smegmatis*, B11, Triacylglycerol, Cell wall permeability, Biofilms

[†]Zhuhua Wu and Weillong Liu contributed equally to this work

*Correspondence:
Huizhong Wu
1627639699@qq.com
Jing Liang
13999641@qq.com
Xunxun Chen
grace_chen514@163.com

[1]Key Laboratory of Translational Medicine of Guangdong, Center for Tuberculosis Control of Guangdong Province, Guangzhou, Guangdong, China
[2]The Sixth People's Hospital of Dongguan, Dongguan, Guangdong, China
[3]Institute of Hepatology, Shenzhen Third People's Hospital, Shenzhen, Guangdong, China
[4]School of Basic Medical Sciences, Guangzhou Health Science College, Guangzhou, Guangdong, China

Background

The unique cell wall structure of *mycobacterium* contributes to its resilience against the host immune system. Multiple cell wall lipids enhance impermeability, intrinsic resistance, persistence within macrophages, virulence, and adaptability to the host environment during infection [1]. Understanding the implications of outer membrane construction for cellular fitness and survival can offer insights into drug development and TB treatment [2].

Mycobacterium can adapt to changing environments and persist within the host due to its capacity to remodel metabolism and resist antibiotics [3]. Triacylglycerol (TAG), a glycerol triester with fatty acids, serves as a major carbon and energy source for *M. tuberculosis* during prolonged infection [4]. TAG accumulates in two forms: synthesized and stored in the bacterial cytoplasm, and present in the mycobacterial cell wall [5]. Cytoplasmic TAG in intracytoplasmic lipid inclusions (ILIs) confer phenotypic drug tolerance and promote pathogen survival [6, 7]. Various factors, including hypervirulent *M. tuberculosis* strains, lipid-rich diets, and environmental stresses, induce ILI formation in mycobacteria [8–10]. Altered biofilms associated with reduced mycolic acid wax ester and long-chain TAG levels play crucial roles in adaptive immune pressure and non-replicating persistence [11].

Small RNAs (sRNAs), typically 50–300 nt in length, are essential molecules involved in regulatory processes [12]. While extensively studied in gram-negative bacteria, knowledge of sRNA functions and regulatory mechanisms in high G + C bacteria, such as *M. tuberculosis* and *M. smegmatis*, remains limited [13, 14]. As novel sRNAs are discovered and their biological functions elucidated, their role as key post-transcriptional regulators of gene expression becomes increasingly evident.

B11 of *M. tuberculosis* (ncRv13660c, MTS2822, 6 C) is approximately 95 nucleotides long and is situated in the intergenic region between Rv3660c and Rv3661, exhibiting a conserved secondary structure featuring two C-rich loops [14]. Its structure suggests a potential role as a structural or protein-binding RNA [15]. Initially identified in 2009 by Arnvig et al., B11 demonstrates increased expression in response to H_2O_2 [16]. While overexpression of B11 in *M. tuberculosis* proves lethal to the bacterium, its overexpression in *Mycobacterium smegmatis* (*M. smegmatis*) leads to slow growth [14]. Disruption of B11 in *Mycobacterium kansasii* correlates with alterations in colony morphology and biofilm formation [17], while its absence in *M. abscessus* results in heightened virulence and pro-inflammatory immune signaling [18]. In *M. smegmatis*, B11 of *M. tuberculosis* binds to panD and dnaB mRNA via C-rich loops, implicating it in various cellular processes [14], suggesting a potential role in cell division regulation. However, the biological functions of B11 and its regulatory processes, especially regarding the regulation of cell wall biosynthesis, still require further in-depth study.

M. smegmatis shares over 2000 homologous genes with *M.tuberculosis* [19]. Its unique cell wall structure is akin to that of *M. tuberculosis* and various other mycobacterial species [20]. Consequently, *M. smegmatis* has been employed as a model organism to investigate the molecular, physiological, and drug resistance mechanisms of *M.tuberculosis*. In this study, we conducted a comprehensive analysis of B11 from *M.tuberculosis* using *M. smegmatis* as a model strain. We found that B11 overexpression affects bacterial growth and colony morphology, increases antibiotic sensitivity and sodium dodecyl sulfate (SDS) surface stress, decreases intracellular survival, and suppresses cytokine secretion in macrophages. Through RNA-seq and lipidomics analysis, we characterized the regulatory and metabolic pathways modulated by B11, particularly affecting TAG accumulation. Additionally, transmission electron microscopy (TEM) revealed a reduction in cell wall thickness associated with B11 overexpression, along with diminished biofilm formation and altered cell wall permeability. Furthermore, we observed that while B11 regulates certain target genes, it does not directly bind to proteins.

Results

Mutant isolation and phenotype analysis

Previously [14], reported that the C-rich loops of B11 are required for growth inhibition. To investigate the functions of B11, the RNAfold program was employed to predict the secondary structure of *M. tuberculosis* B11 (Fig. 1A). To assess the criticality of these C-rich loops for function, mutations were introduced in this region of L2 and L3 (C-to-A conversion at C-rich sequences) (Fig. 1B). Results indicated that Ms_B11 exhibited a smooth phenotype on a solid medium (Fig. 1C). Furthermore, the Ms_B11 strains displayed significantly decreased sliding motility (Fig. 1D). Compared to the control strain (Ms_vc), Ms_B11 began to show reduced growth (Fig. 1E). SEM examination revealed that Ms_B11 strains were significantly elongated compared to the control cells (Fig. 1F). Additionally, Ms_B11 strains exhibited significantly increased cell lengths (2.01 ± 0.85 μm) compared to control strains (1.32 ± 0.56 μm) (Fig. 1G). We also observed that the cell lengths were partially recovered in the Ms_B11 L2 and Ms_B11 L3 strains (1.67 ± 0.73 μm, 1.64 ± 0.59 μm, respectively) (Fig. 1G).

Overexpression of B11 enhances antibiotic sensitivity and SDS surface stress

Subsequently, we examined the susceptibility to vancomycin and linezolid, which target bacterial cell wall assembly and protein synthesis, respectively. The B11

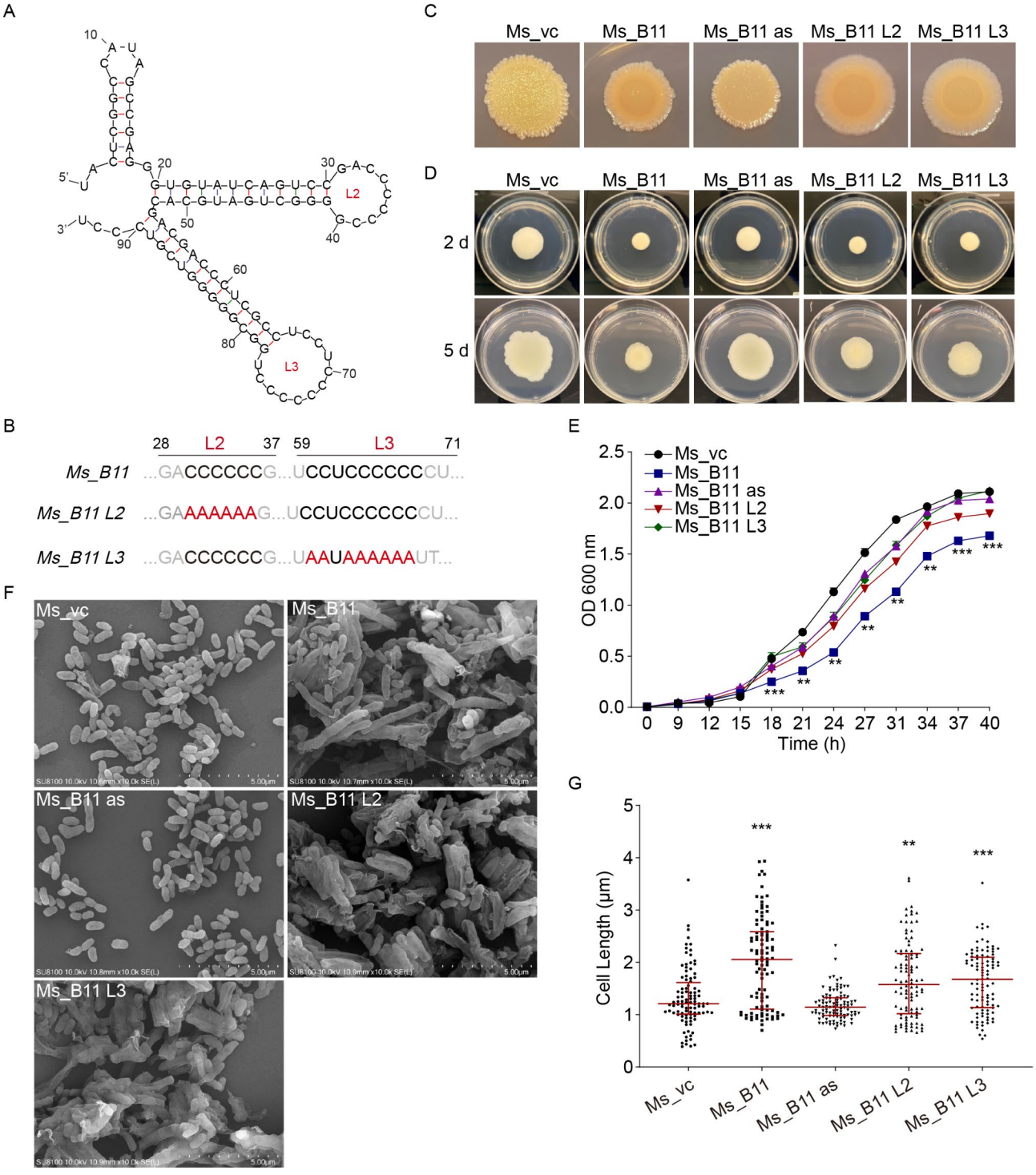

Fig. 1 Mutant isolation and phenotype analysis. (**A**) Prediction of the secondary structure of *M. tuberculosis* B11 using MFold. (**B**) Schematic representation of site-directed mutagenesis in L2 and L3 of B11, with red indicating the mutation sites. (**C**) Colony morphology, (**D**) Sliding motility, and (**E**) Growth curve of recombinant strains. (**F**) Morphology of recombinant strains observed under SEM. (**G**) Calculation of cell lengths from representative fields (approximately 100 cells) as visualized by SEM. The cell length was calculated using ImageJ. A total of 100 cells from multiple fields of view were randomly selected and measured. Lengths of the bacterial cells were calculated from the coordinates of both ends of the cell as measured from representative fields as visualized by SEM. *$P < 0.05$, **$P < 0.01$, ***$P < 0.001$. Ms_vc, *M. smegmatis* harboring empty vector as the control. Ms_B11, *M. smegmatis* expressing B11. Ms_B11 as, *M. smegmatis* expressing B11 antisense. Ms_B11 L2, *M. smegmatis* expressing B11 with site-directed mutagenesis in the L2 loop. Ms_B11 L3, *M. smegmatis* expressing B11 with site-directed mutagenesis in the L3 loop

overexpression strain exhibited decreased survival rates when exposed to high concentrations of vancomycin (5 μg/mL) and linezolid (1 μg/mL) compared to the empty vector strain ($P < 0.05$; Fig. 2A, B). Furthermore, when subjected to SDS surface stress, the B11 overexpression strain displayed reduced survival rates after exposure to 0.05% SDS for 1 and 5 h (Fig. 2C) compared to the empty vector control. Similar trends were observed with recombinant strains Ms_B11 and Ms_vc incubated with 0.05% SDS at varying intervals: the bacterial count in all recombinant strains exposed to 0.05% SDS decreased rapidly, with the B11 overexpression strain showing heightened sensitivity to SDS compared to the empty vector control (Fig. 2D).

Overexpression of B11 reduces intracellular survival and suppresses cytokine secretion in macrophages

To assess whether B11 overexpression affects *M. smegmatis* survival within host cells, we infected THP-1-derived macrophages with the B11 overexpression and control strains. The B11 overexpression strain exhibited decreased intracellular survival during THP-1-derived macrophage infection (Fig. 3A). To evaluate the impact of B11 overexpression on pro-inflammatory cytokines in macrophages, the levels of TNF-α, IL-1β, and IL-6 were measured by ELISA. The supernatant of THP-1-derived macrophages infected with the B11 overexpression strain displayed lower levels of TNF-α ($P = 0.002$) (Fig. 3B), IL-1β ($P = 0.02$) (Fig. 3C), and IL-6 ($P = 0.03$) (Fig. 3D) compared to those infected with the empty vector control.

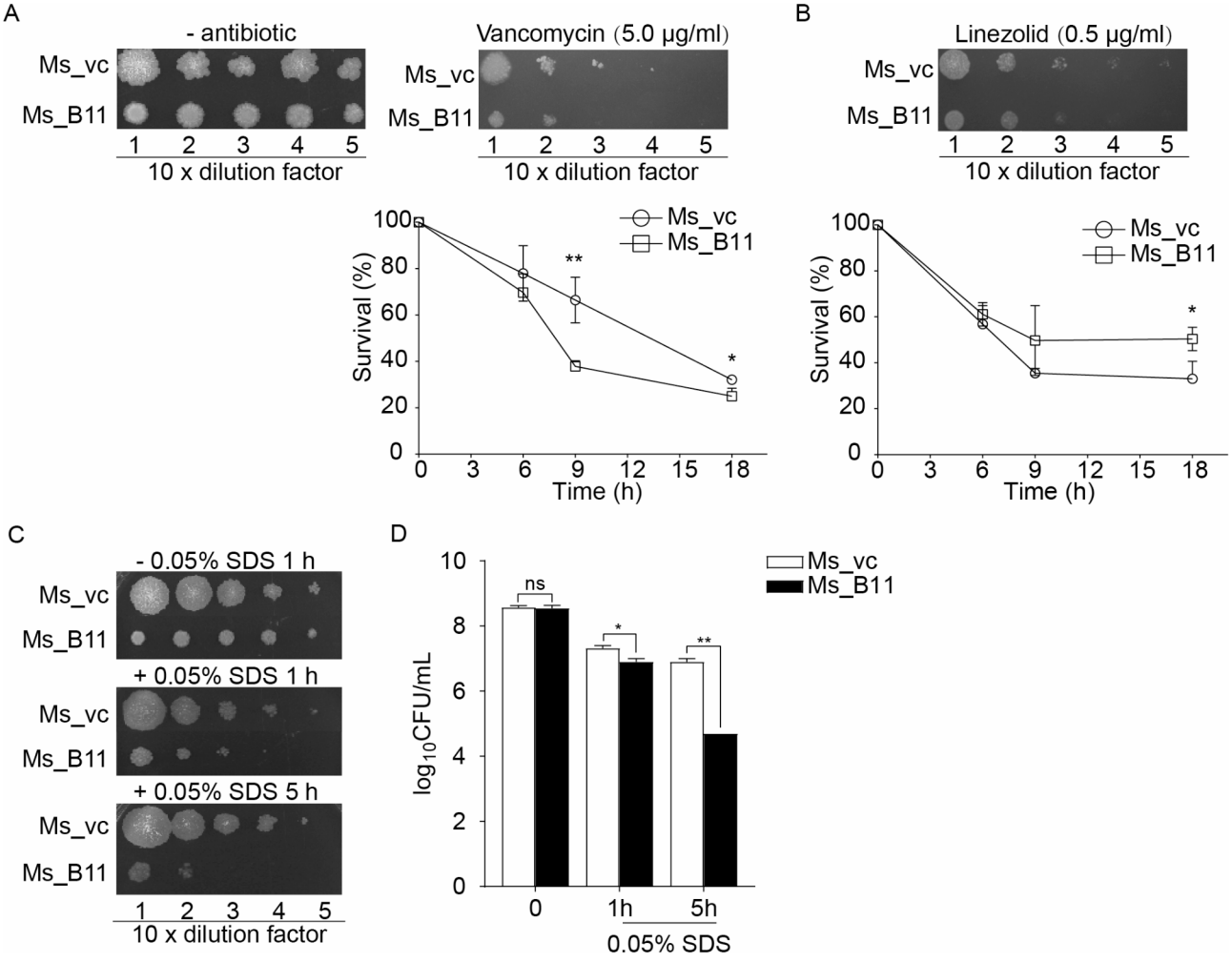

Fig. 2 Overexpression of B11 increases antibiotic sensitivity and SDS surface stress. (**A**) Survival of recombinant strains under indicated concentrations of vancomycin. (**A**) Survival of recombinant strains under indicated concentrations of linezolid. (**C**, **D**) Susceptibility of recombinant strains to 0.05% SDS. (**C**) Recombinant strains treated with 0.05% SDS for either 1–5 h, with 10-fold serial dilutions of recombinant strains spotted on 7H10 medium. The images were taken from different plates. (**D**) Determination of colony-forming units (CFU) at 1, 3, and 5 h

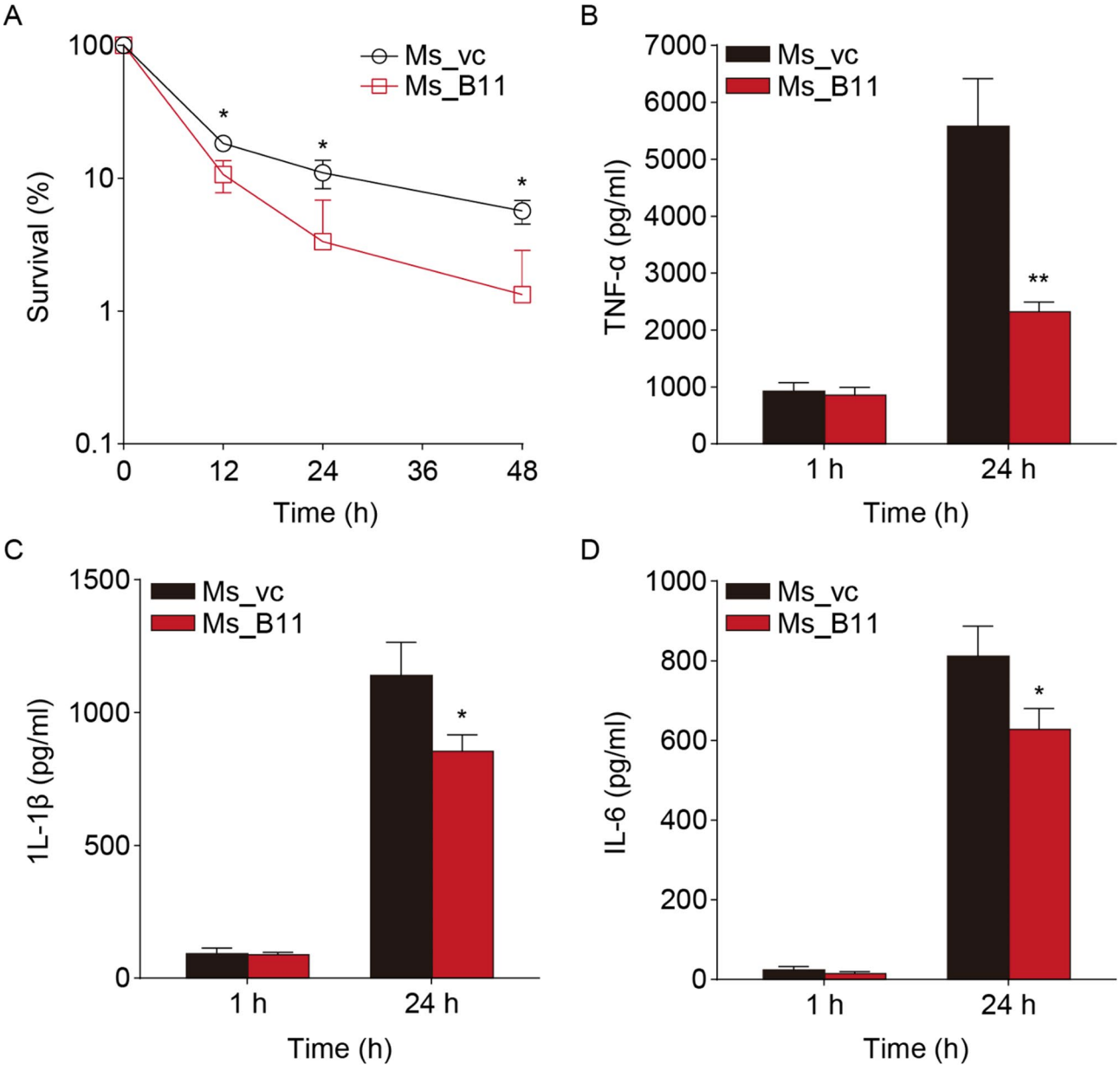

Fig. 3 Overexpression of B11 decreased intracellular survival and suppresses cytokine secretion in macrophages. (**A**) Intracellular survival of recombinant strains within PMA-differentiated macrophages THP-1. Macrophages were infected with recombinant strains at an MOI of 10, followed by washing, lysing, and plating on 7H10 medium to determine bacterial numbers. (**B**) Measurement of cytokines released by macrophages after 24 h of infection with recombinant strains. (*$P < 0.05$; **$P < 0.01$)

B11 modulates TAG accumulation in M. smegmatis

To elucidate the regulatory and metabolic alterations induced by B11 overexpression in *M. smegmatis*, we conducted RNA-seq and lipidomics analyses. A total of 1,300 DEGs were identified in the B11 overexpression strain, comprising 785 upregulated and 515 downregulated genes (Fig. 4A, Supplementary Table 2). Gene Ontology analysis revealed significantly upregulated genes involved in cellular aromatic compound metabolic processes (Biological Process, BP), integral membrane component (Cellular Component, CC), and NADH dehydrogenase (ubiquinone) activity (Molecular Function, MF) in the B11 overexpression strain (Fig. 4B). Conversely, significantly downregulated genes were associated with DNA replication (BP), cytoplasmic localization (CC), and ATP binding (MF) (Fig. 4C). Kyoto Encyclopedia of Genes and Genomes (KEGG) pathway analysis indicated that glycerolipid metabolism was predominantly enriched by upregulated genes in Ms_B11 strains (Fig. 4D), while mismatch repair pathways were most enriched by downregulated proteins (Fig. 4E). Additionally, numerous metabolic enzymes involved in glycerolipid metabolism were

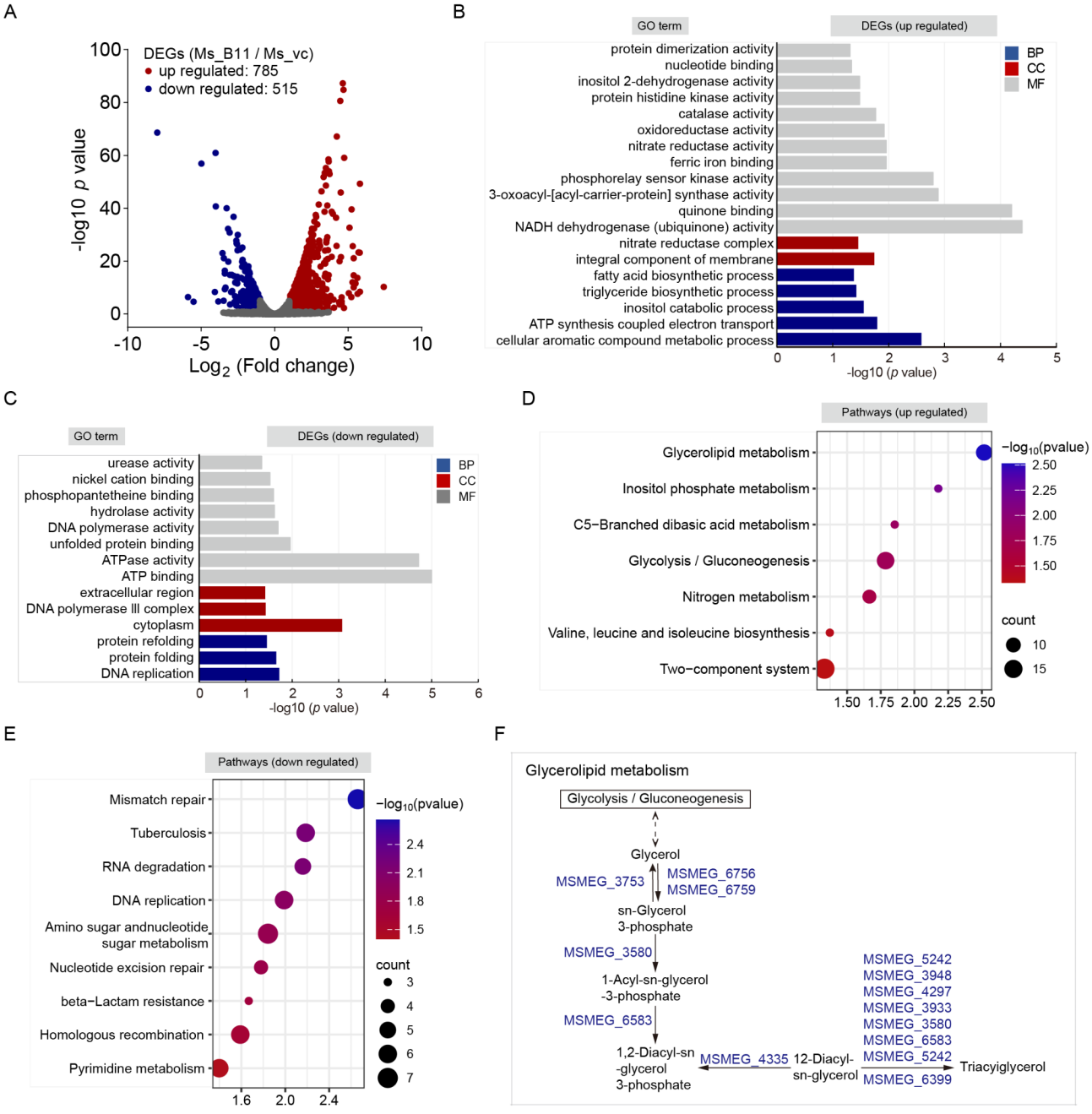

Fig. 4 Transcriptome analysis. (**A**) Volcano plots showing differentially expressed genes between B11-overexpressing and control *M. smegmatis* strains. (**A**, **D**) GO terms and KEGG pathways of upregulated genes. (**C**, **E**) GO terms and KEGG pathways of downregulated genes. (**F**) Identification of glycerolipid metabolism as the most significantly enriched pathway in KEGG analysis. CC, Cellular Component; BP, Biological Process; MF, Molecular Function

accumulated (Fig. 4F), the enzymes involved in these pathways may compete for the same substrate, 1,2-Diacyl-sn-glycerol, which will affect the biosynthesis of TAG. Underscoring the importance of this pathway in non-replicating persistence crucial for *M. smegmatis* survival and re-growth.

Furthermore, comparative lipidomic analyses were conducted to assess differences in lipid profiles between Ms_B11 and Ms_vc strains. Among 10,967 total detected events, 103 met stringent criteria (VIP > 1, $P < 0.05$) (Supplementary Table 4). Notably, a distinct pattern emerged, with 34 events exclusively associated with TAG species (Fig. 5A). Heat map visualization of normalized concentration revealed 103 differential abundances of metabolites (34 events) (Fig. 5B). Individual TAG species, differing in length and unsaturation, were detected at significantly reduced levels in both Ms_B11 and Ms_vc strains (Fig. 5C). Subsequently, we investigated cell

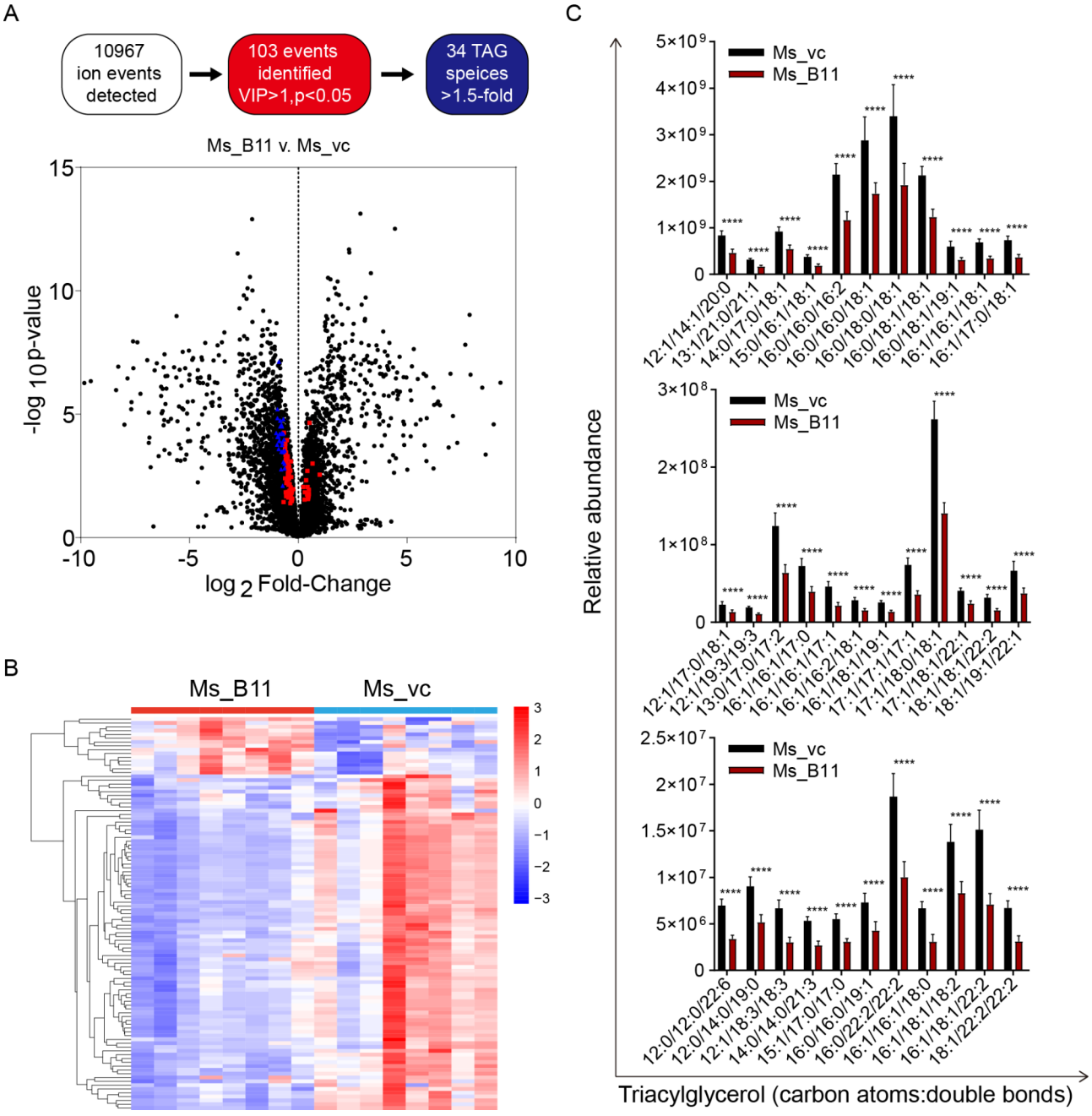

Fig. 5 Lipidomics analysis reveals decreased TAG accumulation upon B11 overexpression. (**A**) Positive mode comparative lipidomics analysis of Ms_B11 and Ms_vc strains resulted in 10,967 total events (black, blue, and red), with 103 metabolites (red) meeting criteria of VIP ≥ 1 and P-value < 0.05. Among them, 34 TAG alkylforms (blue) showed a 1.5-fold increase. (**B**) Hierarchical clustering analysis of the 103 differential metabolites shown in **A**. (**C**) The relative intensities of 34 TAG isoforms in the lipidomics analysis indicate that their abundances have changed significantly. Error bars represent mean ± SD. ****$P < 0.0001$

envelope ultrastructure and lipid inclusions in recombinant strains. *M. smegmatis* cells containing the B11 antisense overexpression vector exhibited ILIs (Fig. 6A, C). The proportion of cells with ILI profiles was more than halved in Ms_B11 compared to control strains (Fig. 6D).

Overexpression of B11 alters cell envelope structure and biofilm formation

To delve deeper into the impact of B11 on bacterial cell envelopes, we examined the ultrastructural features of control and recombinant strains using TEM. The cell envelope exhibited a triple-layered structure comprising the electron-dense outer layer, electron-transparent layer

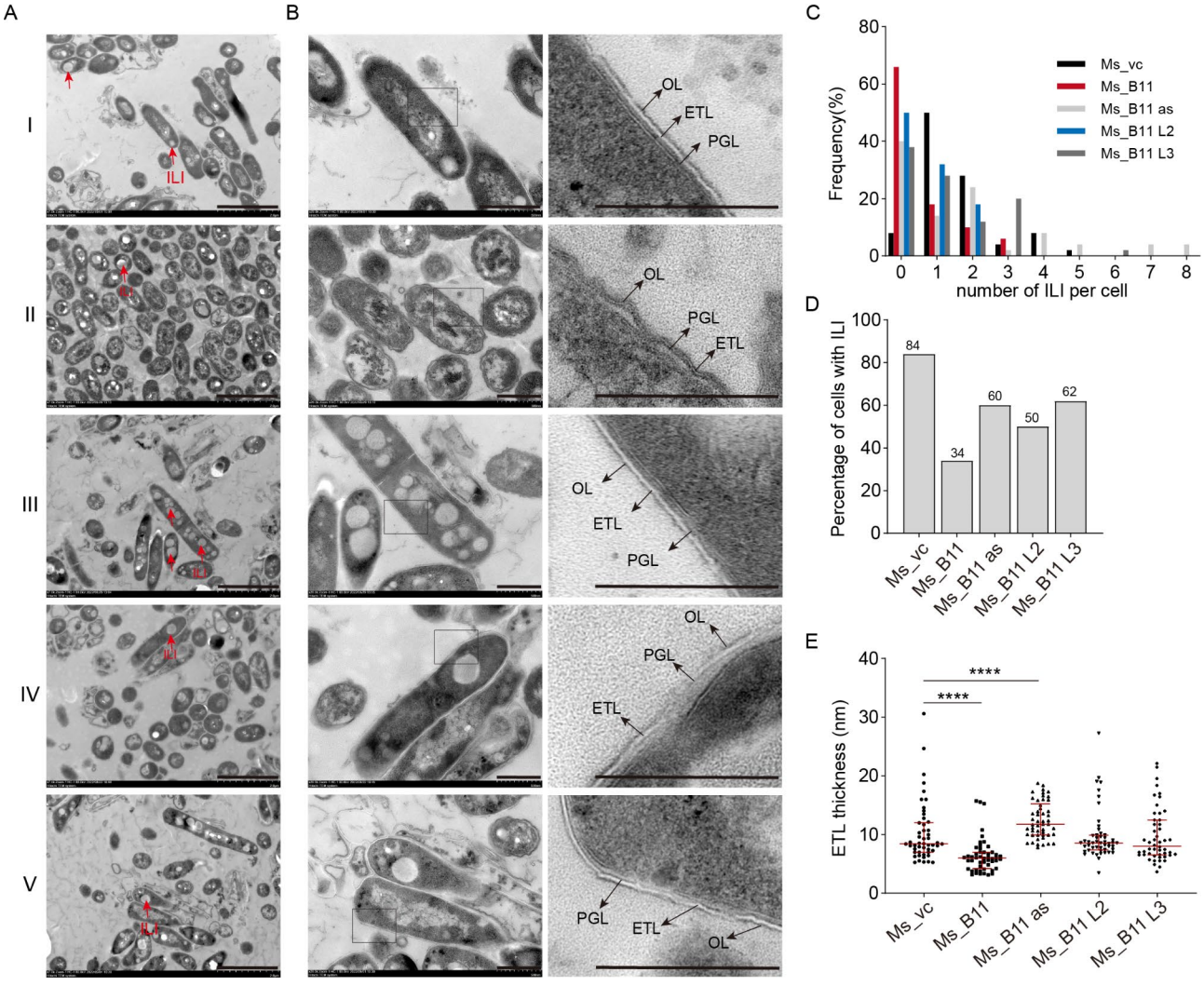

Fig. 6 Cellular ultrastructure analysis of recombinant strains. (**A**) TEM images of recombinant strains depicting ILIs. Scale bar = 2 μm. (**B**) TEM images illustrating detailed ultrastructure of cell envelope layers: outer layer (OL), electron-transparent layer (ETL), and peptidoglycan layer (PGL). Scale bar = 500 nm. (**C**) Quantification of the average number of ILIs per cell. (**D**) Percentage of cells containing ILI. E. Measurement of cell envelope ETL thickness between recombinant strains. Measurements were taken from 50 cells of each strain. I: Ms_vc, II: Ms_B11, III: Ms_B11 as, IV: Ms_B11 L2, V: Ms_B11 L3

(ETL), and peptidoglycan layer (PGL) (Fig. 6B). Notably, the ETL thickness differed significantly between Ms_B11 (6.38 ± 2.89 nm) and Ms_vc (10.27 ± 5.05 nm) strains, with the B11 overexpression strain showing a marked increase (12.46 ± 3.07 nm) (Fig. 6E).

Given the association between biofilm formation and cellular lipid profiles reported in various studies [5], we explored whether B11 overexpression and reduced TAG accumulation impact biofilm formation. The Ms_B11 strain exhibited significantly diminished biofilm growth and less structured pellicle compared to the control strain, a trend also observed in the Ms_B11 L2 and Ms_B11 L3 strains (Fig. 7A). Consistently, crystal violet staining revealed a notable decrease in biofilm signal intensity in the B11 overexpression strain relative to control strains (Fig. 7B).

To assess whether B11 overexpression affected cell wall permeability in *M. smegmatis*, we measured the accumulation rates of fluorescence dyes, EtBr, and Nile Red in Ms_B11 and Ms_vc strains. EtBr accumulation was significantly higher in the Ms_B11 strain compared to the control strain (Fig. 7C). Moreover, Nile Red dye, a lipid stain, exhibited increased uptake in the B11 overexpression strain relative to the control strain (Fig. 7D).

B11 indirectly modulates target genes

The functional mechanisms of noncoding RNAs often involve direct and indirect interactions with RNA-binding proteins. Therefore, we conducted RNA pull-down assays in B11-overexpressing *M. smegmatis* strains using both control and B11 probes. Mass spectrometry identified 49 proteins (emPAI > 1) associated with B11,

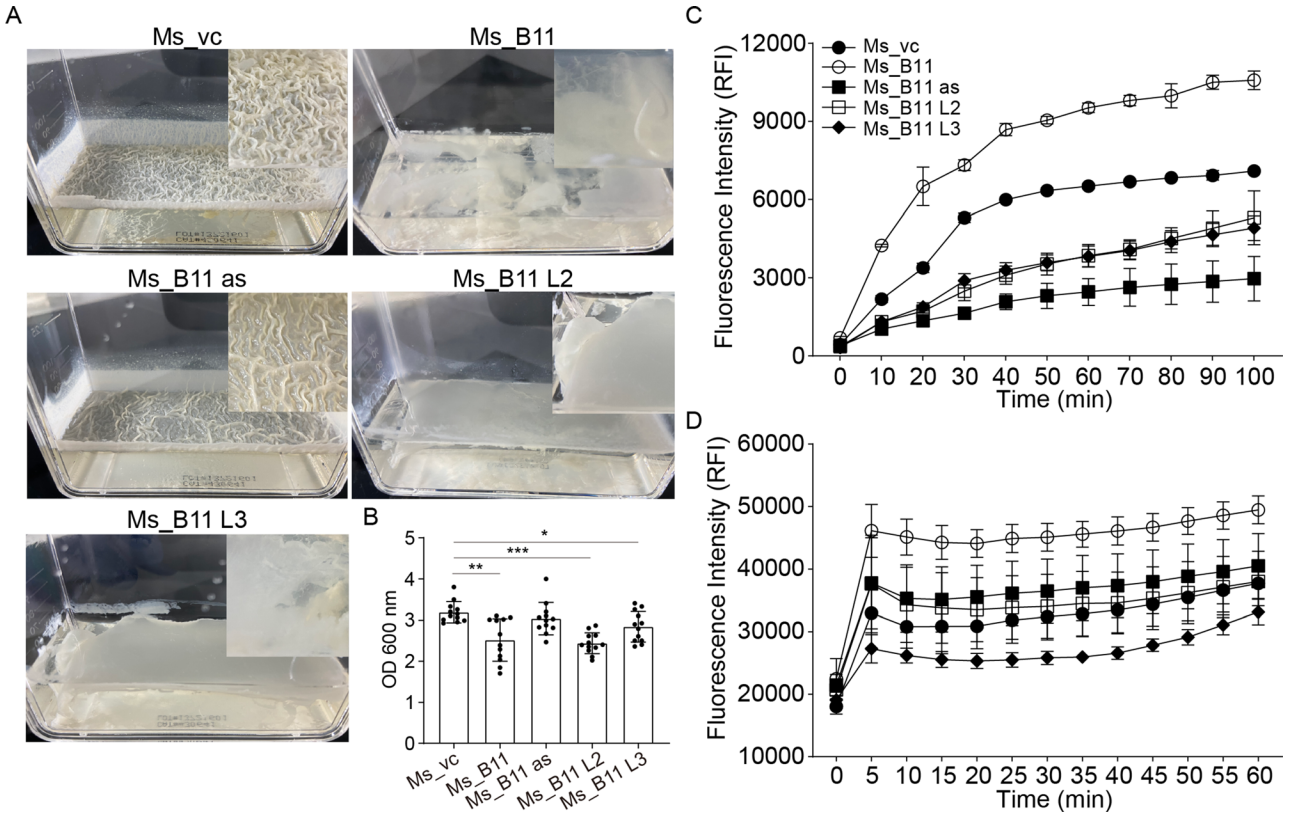

Fig. 7 Overexpression reduces biofilm formation and alters cell wall permeability. (**A**) Effect of B11 on biofilm formation of *M. smegmatis*. Recombinant strains were cultured in Sauton's medium without shaking. (**B**) Quantification of biofilm formation after crystal violet staining. Values are shown as mean ± SD ($n = 12$). (**C**) Mid-log-phase cultures of recombinant strains incubated in phosphate-Buffered Saline containing Tween 20 (PBST) containing 2 μg/ml ethidium bromide (EtBr). (**D**) Mid-log-phase cultures of recombinant strains incubated in PBST containing 20 μM Nile red. RFI, relative fluorescence intensity. *$P < 0.05$, **$P < 0.01$, ***$P < 0.001$

including accC, rpsB, hspX, SecA, and MSMEG_6518 (Fig. 8A, Supplementary Table 3). Combining transcriptome sequencing data, we observed significant upregulation and downregulation ($P < 0.05$) of a group of genes in the B11-overexpressed strain (Fig. 8B). To validate some of these expression changes, qRT-PCR was performed on RNA from the Ms_B11 strain. The relative expression levels of hspX were significantly upregulated compared to the control group, while the expression of rpsB, MSMEG_6092, and rplJ was significantly downregulated (Fig. 8C). Further confirming the direct interaction, three recombinant *M. smegmatis* strains, Ms_hspX, Ms_rplJ, and Ms_6092 strains, were successfully constructed (Fig. 8D). However, RNA pull-down results demonstrated that B11 did not directly bind to these three proteins (Fig. 8E).

Discussion

A pivotal aspect of TB pathogenesis is *M. tuberculosis*'s ability to withstand diverse environmental stressors. Regulatory mechanisms triggered by stress play crucial roles in bacterial survival processes, including colony morphology, physiological adaptations, virulence, and antibiotic resistance. In most bacteria, survival mechanisms, such as the unique cell wall structure of mycobacteria acting as a permeable barrier, are tightly regulated at multiple levels. However, only a few reports have elucidated the physiological role of sRNAs, especially concerning survival under stressful conditions. In this study, we conducted a comprehensive investigation of B11 in *M. smegmatis*. B11 influenced cell wall morphology and TAG accumulation, potentially accounting for the observed growth and colony morphology changes in Ms_B11. The distinctive cell wall structure serves as a protective barrier against environmental stresses such as surface stress SDS and antibiotics. As anticipated, the recombinant Ms_B11 phenotype exhibited greater sensitivity to SDS surface stress, vancomycin, and linezolid compared to Ms_vc, suggesting a role for B11 in stress response. In this study, we found that B11 overexpression affects bacterial growth and colony morphology, increases antibiotic sensitivity and sodium dodecyl sulfate (SDS) surface stress, decreases intracellular survival, and suppresses cytokine secretion in macrophages. Furthermore, the noticeable decrease in TAG buildup resulting from the overexpression of B11 is consistent with

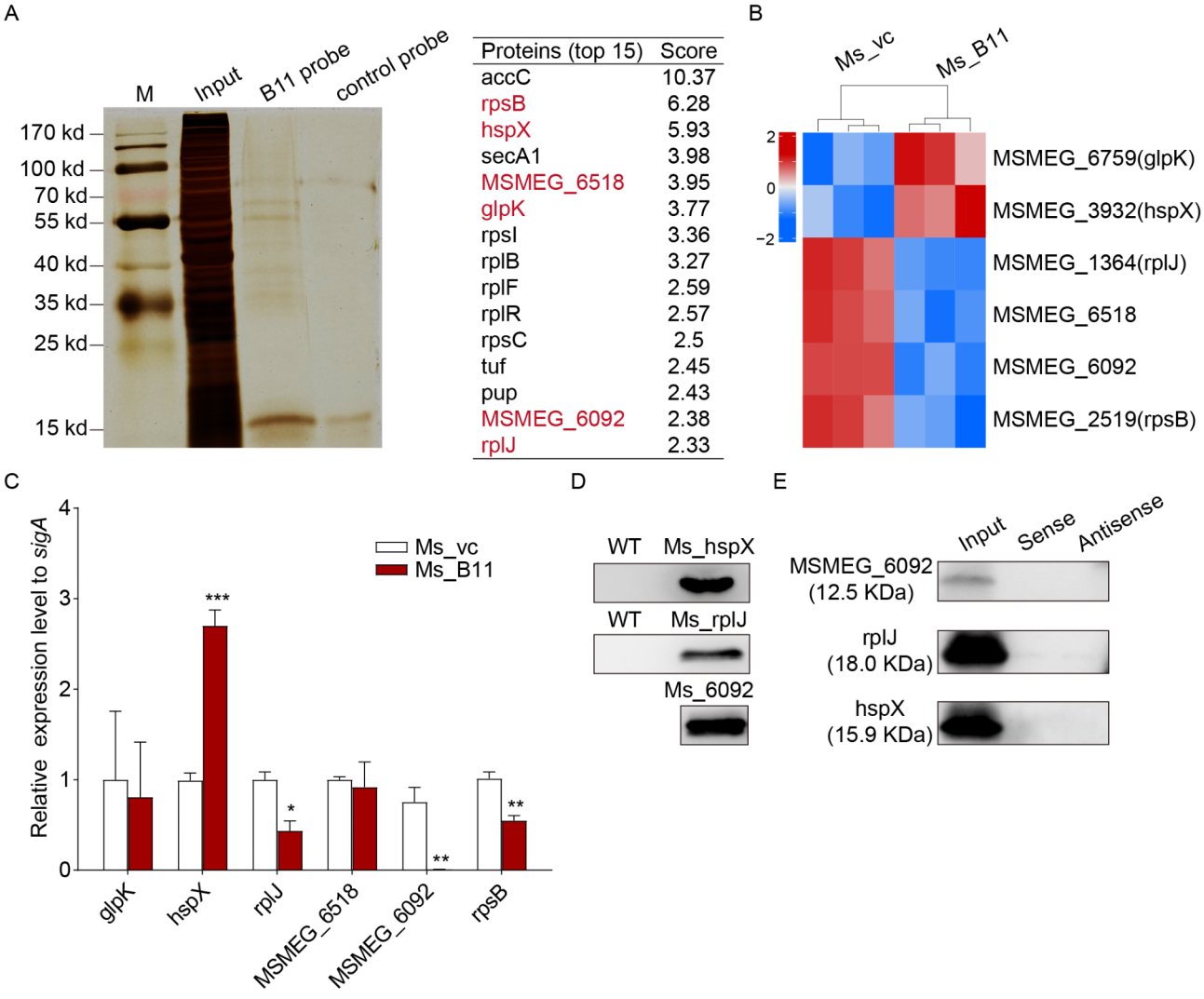

Fig. 8 B11 indirectly regulates target genes without direct binding to proteins. (**A**) Identification of B11-binding proteins. Left: silver staining of pulled-down proteins. Right: mass spectrometry showing the top 10 proteins pulled-down by the B11 probe. (**B**) Heat map illustrating differentially expressed genes in RNA-seq dataset. Red indicates highly expressed genes; blue, lowly expressed genes. (**C**) qRT-PCR analysis verifying the expression of genes corresponding to B11-binding proteins. *$P<0.05$, **$P<0.01$, ***$P<0.001$. (**D**) Expression of hspX, rpiL, and MSMEG_6092 in *M. smegmatis*. Western blot images showing the expression of flag-tagged protein. (**E**) Biotinylated B11 or antisense RNA incubated with whole-cell lysates from hspX, rpiL, or MSMG_6092 overexpression strains. Membranes immunoblotted for hspX, rpiL, and MSMG_6092. Input, total protein group

variations in the cell wall's permeability and its increased thickness, which probably plays a role in the displayed resistance to vancomycin and linezolid, also leads to the alteration of the phenotype.

According to previous studies, B11 appears to play a role in growth and colony morphology in bacteria, including *M. tuberculosis*, *M. smegmatis* [16], and *M. kansasii* [17]. Here, we utilized *M. smegmatis* mc^2155 as our model to gain insights into the cellular function of B11. Our findings are consistent with previous reports: the expression of B11 resulted in slow growth and altered colony morphology, along with changes in cell wall-associated properties [14, 16]. The transition from rough to smooth colony morphology is closely associated with bacterial biofilm formation [21]. Congo red, an amphiphilic dye that binds to lipoproteins, was employed to assess the overall hydrophobicity of the mycobacterial cell wall [22]. Cell wall hydrophobicity is intricately linked to bacterial aggregation and biofilm formation. In our study, Congo red staining revealed significant differences between the B11 overexpression strains and the control strains. The altered Congo red staining of Ms_B11 colonies could also account for the impaired biofilm formation, which was further confirmed in a liquid medium. The abnormal Congo red staining and reduced biofilm formation of Ms_B11 colonies suggest that overexpression of B11 may inhibit biofilm formation. The early stage of bacterial biofilm formation is the adhesion

and aggregation of microbial cells [23]. However, the SEM results of Ms_B11 and mutants show significant aggregation compared to vector control and antisense strains. The formation of pellicles, biofilms, and cords is a complex and dynamic process that involves multiple factors, including cell-cell interactions, extracellular matrix components, and environmental conditions. At this specific phase, bacteria are capable of either loosely clustering together or splitting off into the planktonic state [24]. It is likely that B11 and its mutants have had an impact on the expression of particular essential genes responsible for governing biofilm synthesis. Additionally, our findings reveal that the B11-overexpressing strains possess cell wall imperfections and a decreased TAG synthesis. As a result, even while aggregation is in progress, the surface attributes of the cells may be modified correspondingly, which in turn has an adverse effect on the biofilm formation process. Upon conducting the functional analysis, we found that L2 and L3 exhibited phenotypes quite similar to Ms_B11, albeit not identical. This indicates that L2 and L3 are integral to the functioning of B11, although the exact mechanism involved calls for additional investigation.

Our further investigations into the cell lipid profiles revealed significant alterations in TAG accumulation in B11-overexpressed strains, indicating changes in ILI accumulation and cell wall integrity. TAG serves as the primary energy reservoir in *Mycobacterium*, accumulating in large quantities within cytoplasmic ILIs [5]. Here, we have confirmed that B11 can decrease TAG accumulation in *M. smegmatis*. Additionally, previous studies have reported substantial amounts of TAG in the outer membrane of *M. smegmatis* [25]. Our ultrastructural analysis revealed cell wall defects in B11-overexpressed strains, characterized by a significant reduction in the ETL, suggesting a potential impact on TAG accumulation within the cell wall. ETL is a distinct and significant component of the mycobacterial cell envelope structure. It is is chiefly constituted by lipids such as mycolic acids [26]. Studies have shown that oxidative stress, iron deficiency and exposure to isoniazid reduce the thickness of the ETL of the cell envelope [10]. Prior research has underscored the significance of TAG in antibiotic tolerance and survival within lipid-rich environments [5, 27]. Specifically, ILI accumulation has been associated with phenotypic drug tolerance [28]. Consistent with these findings, our results demonstrate increased susceptibility of B11-overexpressed *M. smegmatis* to vancomycin and linezolid, indicative of reduced TAG accumulation. Moreover, we observed decreased intracellular survival of B11-overexpressed strains during macrophage infection. We provided evidence indicating that B11 overexpression leads to suppression of cytokine secretion, including TNF-α, IL-1β, and IL-6, in macrophages. While cytoplasmic TAG within ILIs may promote pathogen survival during dormancy and reactivation [5], the function of TAG accumulating on the cell wall remains unclear. Further investigation is warranted to elucidate the potential relationship between TAG accumulation and resistance or survival mechanisms. In summary, our findings suggest that B11 overexpression impacts TAG accumulation in *M. smegmatis*, influencing antibiotic tolerance and survival during macrophage infection.

Furthermore, our study revealed that B11 impacts cell wall permeability. The uptake of EtBr and Nile red has been utilized to assess mycobacterial cell wall permeability [22]. Previous research has linked the uptake of EtBr and Nile red to the lipid composition of the cell wall [29]. Here, we demonstrated for the first time, to our knowledge, that B11 alters cell wall permeability, evidenced by increased uptake of EtBr and Nile red. SDS serves as a valuable tool to investigate perturbations in the cell membrane/cell wall [30]. Notably, the survival capacity of Ms_B11 under SDS exposure was significantly diminished compared to control strains, indicating a cell wall defect in Ms_B11. Studies have underscored the significant impact of cell membrane permeability on drug penetration [31]. Decreased permeability of the bacterial cell wall can hinder antibacterial drug penetration [32]. Our experimental findings revealed that the B11 overexpression strain exhibited reduced survival following exposure to high concentrations of vancomycin and linezolid compared to the empty vector strain. This observation, suggesting a role for B11 in resistance to these two drugs, is particularly notable. Consistently, previous reports have indicated that B11 deletion mutants led to increased resistance to linezolid in *M. abscessus* [18]. Collectively, our results indicate that B11 influences survival under various in vitro stresses, including surface stress SDS and exposure to multiple antibiotics. Consequently, bacterial stress responses may contribute to the development of antibiotic resistance in bacteria exposed to stressful conditions [33]. However, a more comprehensive understanding of the impact of mycobacterial stress on antibiotic resistance warrants further investigation.

Previous research findings have shown that B11 is a regulator of genes involved in multiple cellular functions, including DNA replication [14]. In our study, genes related to DNA metabolism and ribosomal proteins appear downregulated. Some ribosomal proteins also appear in the pull-down experiment. DNA replication is a fundamental process for bacterial proliferation [34]. The downregulation of DNA replication appears to be a crucial factor contributing to both the observed bacterial growth retardation and the reduction in membrane formation in our study, and further investigations are needed to fully elucidate the complex molecular mechanisms underlying these relationships. Additionally,

our findings suggest that B11 negatively regulates certain genes but does not directly bind to proteins. It is established that sRNAs can modulate gene expression by directly binding to mRNA sites. Previous studies have reported that the C-rich loops of B11 base-pair with panD mRNA independently of RNA chaperones, although G-rich stretches were not identified in other validated targets (MSMEG 0408 and mce1F) [14]. Further research is required to elucidate whether novel classes of RNA chaperones modulate the activity of B11. Despite the significant findings in this study regarding the influence of B11 on *M.smegmatis*, several limitations must be acknowledged. Regarding the mechanism of action, the study's exploration of how B11 modulates TAG accumulation remains somewhat superficial. Although connections between B11 overexpression and alterations in glycerolipid metabolism genes and enzymes have been established, the precise molecular interactions and regulatory cascades are yet to be fully deciphered.

Conclusions

In summary, our study highlights the impact of B11 overexpression on *M. smegmatis*, revealing alterations in bacterial growth, colony morphology, and the inhibition of biofilm formation. Additionally, the observed reduction in triglyceride accumulation due to B11 overexpression correlates with changes in cell wall permeability and thickness, likely contributing to the observed phenotypic tolerance to vancomycin and linezolid. However, the precise function of the accumulated TAG on the cell wall remains unclear, presenting a promising avenue for potential drug development targets.

Materials and methods

Bacterial strains and growth conditions

The research utilized *M. smegmatis* mc^2155 and *Escherichia coli* DH5α strains. *M. smegmatis* mc^2155, overexpressing strains, and mutant strains were cultured in Middlebrook 7H9 medium supplemented with 0.2% glycerol, 0.05% Tween 80, and 50 mg/mL of kanamycin when necessary. Middlebrook 7H10 medium supplemented with 2% glycerol was used for culturing *M. smegmatis* mc^2155. *E. coli* DH5α strains were cultured in Luria–Bertani (LB) medium supplemented with 50 mg/mL of kanamycin when required. All cultures were incubated at 37 °C with shaking at 150 rpm.

Molecular cloning and plasmid construction

Supplementary Table 1 provides details of the bacterial strains, plasmids, and primer sequences used for cloning. To assess the criticality of these C-rich loops of B11 for its function, mutations were introduced in this region of L2 and L3 (C-to-A conversion at C-rich sequences). B11 of *M.tuberculos*is, B11 antisense and its mutants were cloned into pMV261 at the HindIII sites. To identify the B11-binding proteins, genes from *M. smegmatis* mc^2155 were PCR-amplified, digested with BamHI and HindIII, and then cloned into pMV261 with an N-terminal 3 × FLAG tag. The resulting plasmids were electroporated into *M. smegmatis* mc^2155 as previously described. DNA sequencing was conducted to confirm all constructs. The expression of proteins in recombinant strains was analyzed via western blotting.

qPCR analysis

Cells were collected and lysed using Fastprep-24 (MP Biomedicals) following the manufacturer's instructions. RNA was harvested using Trizol-based methods as previously described [35]. Briefly, RNA was recovered by centrifugation, phenol-chloroform extraction, and isopropyl alcohol precipitation, and re-suspended in RNase-free H_2O. Subsequently, total RNA was reverse-transcribed to cDNA using ChamQ Universal SYBR qPCR Master Mix (Vazyme Biotech). The mRNA expression of selected genes was analyzed using the same qPCR Master Mix. Mean ± standard error of mean values were calculated from three independent experiments, and significant differences were determined using Student's unpaired t-test. The primer sequences utilized in this study are listed in Supplementary Table 1.

Western blot analysis

The expression of Flag-tagged HspX, RplJ, and MSMEG_6092 was verified using western blotting with a mouse anti-Flag-tag monoclonal antibody (Beyotime, China) as the primary antibody and an HRP-conjugated goat anti-mouse IgG antibody (Beyotime, China) as the secondary antibody. Lysates of recombinant strains were separated using 12% sodium dodecyl sulfate polyacrylamide gel electrophoresis, and proteins were transferred on to polyvinylidene fluoride membranes. The membranes were blocked and then incubated with diluted primary antibodies. Subsequently, membranes were incubated with an HRP-labeled anti-rabbit IgG antibody (Beyotime, China), and the signal was developed using the Bio-Rad ChemiDoc XRS + instrument and image software.

Scanning electron microscopy

Scanning electron microscopy (SEM) was performed according to our published procedure [36]. Briefly, cells were collected and fixed with 2.5% glutaraldehyde overnight at 4 °C. Sequential ethanol dehydrations were performed in a graded series, followed by critical point drying using a Hitachi HCP-2 Critical Point Dryer (Hitachi High-Technologies Corp., Tokyo, Japan). After drying, the samples were sputter-coated, and ultrastructure

examination was conducted using a Zeiss Ultra55 electron microscope.

TEM

TEM was performed according to our published procedure [36]. Cells were harvested, fixed, and dehydrated in a graded ethanol series, then embedded in Spurr resin. Thin sections were examined using a Tecnai Spirit (FEI) transmission electron microscope. Lipid inclusions in the intracytoplasmic space were regularly detected. Cell wall thickness was analyzed using ImageJ software.

Phenotypic analysis

Growth curve analysis, sliding motility assay, Congo Red assay, and biofilm assay were performed as previously described [36]. Bacterial cultures were grown to the exponential phase (OD = 0.2–0.4 at 600 nm). The optical density at 600 nm (OD_{600}) was measured at intervals of 3 h to obtain growth curves. *M. smegmatis* mc^2155 recombinant strains were cultured in LB medium supplemented with 100 mg/mL Congo Red (Sigma), Sauton liquid medium, and 7H9 medium supplemented with 0.3% agar, respectively, and phenotypes were observed.

Spot tests

Recombinant strains were cultured to exponential phase and adjusted to an OD_{600} of 0.2. Ten-fold serial dilutions of recombinant strains were spotted onto 7H10 agar containing the indicated concentrations of SDS (0.05%), vancomycin (5.0 μg/mL), and linezolid (μg/mL).

Survival curves

Survival curve analysis was conducted as previously described [37]. Briefly, cultures of recombinant strains at mid-exponential phase were first diluted in 7H9 medium and incubated at 37 °C. Subsequently, they were treated with diverse concentrations of antibiotics as specified. SDS was introduced to reach a final concentration of 0.05% in the recombinant strain cultures, which were further incubated at 37 °C. After indicated time, bacterial survival was quantified by colony formation on drug-free agar.

Macrophage infections and cytokine assays

The human leukemia monocytic cell line (THP-1) was utilized for this study. THP-1 macrophages were infected with recombinant strains at a multiplicity of infection (MOI) of 10:1. For the intracellular bacterial survival assay, cells were washed, lysed, serially diluted, and inoculated onto 7H10 agar. The supernatant of each culture was collected and analyzed for cytokine levels using an enzyme-linked immunosorbent assay (ELISA) kit (Beyotime).

RNA-Seq analysis

Total RNA was extracted from recombinant strains and used for sequencing library construction. The Ultra-™Directional RNA Library Prep Kit for Illumina (NEB) was employed according to the manufacturer's instructions. The final library products were purified and assessed using an Illumina second-generation high-throughput sequencing platform at Allwegene Technology Inc., Beijing. These clean reads were then mapped to the reference genome sequence (*Mycobacterium smegmatis* MC^2155) by Bowtie2 v2.2.6. Corrected P-value of 0.05 and absolute value of log2 (Fold change) greater than 1 were set as the threshold for significantly differential expression. Three biological replicates were used for each group.

RNA pull-down assays and mass spectrometry (MS) anaysis

The full-length sense RNA of B11 was biotin-labeled using the Pierce™ RNA 3′ End Desthiobiotinylation Kit (BersinBio). Pull-down assays were performed by incubating biotin-labeled RNA with cell lysates using the RNA pull-down Kit (BersinBio). This complex could bind to streptavidin-labeled magnetic beads to separate from the other components of incubation solution. To identify the interacting proteins, MS analyses were performed by BersinBio (Guangzhou, China). The Thermo Scientific Q-Exactive Quadrupole-Orbitrap Mass Spectrometer, alongside the Thermo Dionex Ultimate 3000 RSLCnano System, were employed for the analytical procedures. Data acquisition was conducted using Xcalibur software, version 3.0.63.3. Subsequent processing of the MS raw file for protein identification and quantification was carried out with MaxQuant software, version 1.5.2.8.

Lipidomics analysis

Lipidomics analysis was conducted following our previously published protocol [36]. In brief, lipid extraction was performed using a chloroform/methanol solution (2:1, v: v) and an ultrasonic cleaner. The supernatant was then dried using N_2 and dissolved in chloroform/methanol solution (2:1, v: v). Lipid samples were processed and analyzed by Biotree Biotech (Shanghai, China). LC-MS/MS analyses were performed using a Dionex UltiMate 3000 (UHPLC)–Thermo Orbitrap Elite. Raw data were converted to the mz.data format using Agilent MassHunter Qualitative Analysis B.08.00 software (Agilent Technologies, United States), and further processed using the XCMS program. Multivariate analysis was performed using the SIMCA16.0.2 software package (Umetrics, Umea, Sweden).

Ethidium bromide and Nile red uptake assay

The ethidium bromide (EtBr) and Nile red uptake assay were conducted according to a previously established

protocol [38]. Recombinant strains were cultured to exponential phase and adjusted to an OD_{600} of 0.8. Then, 200 µL of bacterial suspension was added in triplicate to a 96-well black fluoroplate and treated with EtBr and Nile red dye to a final concentration of 2.0 µg/mL and 20 µM, respectively. The fluorescence intensity of accumulated dyes was measured on a BioTek Synergy HIM microplate reader (excitation: 544 nm, emission: 590 nm).

Statistical analysis

Data from each group are presented as the mean ± standard deviation (SD). Statistical analysis employed the unpaired Student t test, statistical signifcance was set at $P < 0.05$.

Abbreviations

M. tuberculosis	*Mycobacterium tuberculosis*
TB	Tuberculosis
M. smegmatis	*Mycobacterium smegmatis*
TAG	Triacylglycerol
SDS	Sodium dodecyl sulfate
ILIs	Intracytoplasmic lipid inclusions
sRNAs	Small RNAs
TEM	Transmission electron microscopy
ETL	Electron-transparent layer
PGL	Peptidoglycan layer

Supplementary Information

The online version contains supplementary material available at https://doi.org/10.1186/s12866-025-03826-7 .

Supplementary Material 1

Supplementary Material 2

Acknowledgements
Not applicable.

Author contributions
ZW, XC, JL and HW designed the experiments. ZW, WL, QT, YC, XL JH and HL performed the experiments, analyzed the data, and interpreted the results. ZW and QT wrote the manuscript. The author(s) read and approved the fnal manuscript.

Funding
This study was supported by Dongguan Science and Technology of Social Development Program (No. 202050715005178), the Youth Innovative Talents Project in Colleges and Universities in Guangdong Province (No. 2024KQNCX209), Guangdong Provincial Clinical Research Center for Tuberculosis (No. 2020B1111170014), the Science and Technology Planning Project of Guangdong Province, China (No. 2021B1212030003), the Science and Technology Program of Guangzhou, China (No. 202201011764), and the Special Fund for Science and technology innovation strategy of Guangdong province (No. pdjh2024b632).

Data availability
The RNA - seq data has been submitted to the Sequence Read Archive (https://www.ncbi.nlm.nih.gov/sra/PRJNA1097297) with the bioProject accession number PRJNA1097297. The lipidomics data reported in this paper have been deposited in the OMIX, China National Center for Bioinformation / Beijing Institute of Genomics, Chinese Academy of Sciences (https://ngdc.cncb.ac.cn/omix: accession no.OMIX006976).

Declarations

Ethics approval and consent to participate
Not applicable.

Consent for publication
Not applicable.

Competing interests
The authors declare no competing interests.

Received: 27 July 2024 / Accepted: 13 February 2025
Published online: 08 March 2025

References

1. Sun J, Rutherford ST, Silhavy TJ, Huang KC. Physical properties of the bacterial outer membrane. Nat Rev Microbiol. 2022;20(4):236–48. https://doi.org/10.1038/s41579-021-00638-0.
2. Mi J, Gong W, Wu X. Advances in Key Drug Target Identification and New Drug Development for Tuberculosis. Biomed Res Int. 2022; 2022:5099312. https://doi.org/10.1155/2022/5099312
3. Abo-Kadoum MA, Assad M, Dai Y, Lambert N, Moure U, Eltoukhy A, Nzaou S, Moaaz A, Xie J. Mycobacterium Tuberculosis Raf Kinase Inhibitor Protein (RKIP) Rv2140c is involved in Cell Wall Arabinogalactan Biosynthesis Via Phosphorylation. Microbiol Res. 2021;242:126615. https://doi.org/10.1016/j.micres.2020.126615.
4. Chang D, Guan XL. Metabolic versatility of Mycobacterium Tuberculosis during infection and dormancy. Metabolites. 2021;11(2):88. https://doi.org/10.3390/metabo11020088.
5. Maurya RK, Bharti S, Krishnan MY. Triacylglycerols: fuelling the Hibernating Mycobacterium Tuberculosis. Front Cell Infect Microbiol. 2018;8:450. https://doi.org/10.3389/fcimb.2018.00450.
6. Hammond R, Baron VO, Lipworth S, Gillespie SH. Enhanced methodologies for detecting phenotypic resistance in Mycobacteria. Methods Mol Biol. 2018;1736:85–94. https://doi.org/10.1007/978-1-4939-7638-6_8.
7. Rengarajan J, Bloom BR, Rubin EJ. Genome-wide requirements for Mycobacterium Tuberculosis Adaptation and Survival in macrophages. Proc Natl Acad Sci U S A. 2005;102(23):8327–32. https://doi.org/10.1073/pnas.0503272102.
8. Reed MB, Gagneux S, Deriemer K, Small PM, Barry CR. The W-Beijing lineage of Mycobacterium Tuberculosis overproduces triglycerides and has the DosR Dormancy Regulon Constitutively Upregulated. J Bacteriol. 2007;189(7):2583–9. https://doi.org/10.1128/JB.01670-06.
9. Caire-Brandli I, Papadopoulos A, Malaga W, Marais D, Canaan S, Thilo L, de Chastellier C. Reversible lipid Accumulation and Associated Division arrest of Mycobacterium Avium in Lipoprotein-Induced Foamy macrophages may resemble key events during latency and reactivation of tuberculosis. Infect Immun. 2014;82(2):476–90. https://doi.org/10.1128/IAI.01196-13.
10. Vijay S, Hai HT, Thu D, Johnson E, Pielach A, Phu NH, Thwaites GE, Thuong N. Ultrastructural analysis of Cell Envelope and Accumulation of lipid inclusions in clinical Mycobacterium tuberculosis isolates from Sputum, oxidative stress, and Iron Deficiency. Front Microbiol. 2017;8:2681. https://doi.org/10.3389/fmicb.2017.02681.
11. Wright CC, Hsu FF, Arnett E, et al. The Mycobacterium tuberculosis MmpL11 cell wall lipid transporter is important for Biofilm formation, intracellular growth, and nonreplicating persistence. Infect Immun. 2017;85(8):e00131–17. https://doi.org/10.1128/IAI.00131-17.
12. Zhou Y, Xie J. The roles of Pathogen Small RNAs. J Cell Physiol. 2011;226(4):968–73. https://doi.org/10.1002/jcp.22483.
13. Taneja S, Dutta T. On a Stake-Out: mycobacterial small RNA identification and regulation. Noncoding RNA Res. 2019;4(3):86–95. https://doi.org/10.1016/j.ncrna.2019.05.001.
14. Mai J, Rao C, Watt J, Sun X, Lin C, Zhang L, Liu J. Mycobacterium Tuberculosis 6 C sRNA binds multiple mRNA targets Via C-rich loops Independent of RNA chaperones. Nucleic Acids Res. 2019;47(8):4292–307. https://doi.org/10.1093/nar/gkz149.
15. Arnvig K, Young D. Non-coding RNA and its potential role in Mycobacterium Tuberculosis Pathogenesis. Rna Biol. 2012;9(4):427–36. https://doi.org/10.4161/rna.20105.

16. Arnvig KB, Young DB. Identification of small RNAs in Mycobacterium Tuberculosis. Mol Microbiol. 2009;73(3):397–408. https://doi.org/10.1111/j.1365-2958.2009.06777.x.
17. Budell WC, Germain GA, Janisch N, McKie-Krisberg Z, Jayaprakash AD, Resnick AE, Quadri L. Transposon Mutagenesis in Mycobacterium Kansasii Links a small RNA gene to Colony Morphology and biofilm formation and identifies 9,885 intragenic insertions that do not compromise colony outgrowth. Microbiologyopen. 2020;9(4):e988. https://doi.org/10.1002/mbo3.988.
18. Bar-Oz M, Martini MC, Alonso MN, et al. The small non-coding RNA B11 regulates multiple facets of Mycobacterium Abscessus Virulence. Plos Pathog. 2023;19(8):e1011575. https://doi.org/10.1371/journal.ppat.1011575.
19. Li Q, Ge F, Tan Y, Zhang G, Li W. Genome-wide transcriptome profiling of Mycobacterium Smegmatis MC(2) 155 cultivated in minimal media supplemented with cholesterol, androstenedione or glycerol. Int J Mol Sci. 2016;17(5):689. https://doi.org/10.3390/ijms17050689.
20. King GM. Uptake of Carbon Monoxide and Hydrogen at environmentally relevant concentrations by Mycobacteria. Appl Environ Microbiol. 2003;69(12):7266–72. https://doi.org/10.1128/AEM.69.12.7266-7272.2003.
21. Uhlich GA, Cooke PH, Solomon EB. Analyses of the Red-Dry-Rough phenotype of an Escherichia Coli O157:H7 strain and its role in Biofilm formation and resistance to Antibacterial agents. Appl Environ Microbiol. 2006;72(4):2564–72. https://doi.org/10.1128/AEM.72.4.2564-2572.2006.
22. Bharti S, Maurya RK, Venugopal U, Singh R, Akhtar MS, Krishnan MY. Rv1717 is a cell Wall - Associated beta-galactosidase of Mycobacterium Tuberculosis that is involved in Biofilm Dispersion. Front Microbiol. 2020;11:611122. https://doi.org/10.3389/fmicb.2020.611122.
23. Zhao A, Sun J, Liu Y. Understanding bacterial biofilms: from definition to treatment strategies. Front Cell Infect Microbiol. 2023;13:1137947. https://doi.org/10.3389/fcimb.2023.1137947.
24. Kumar A, Alam A, Rani M, Ehtesham NZ, Hasnain SE. Biofilms: Survival and Defense Strategy for pathogens. Int J Med Microbiol. 2017;307(8):481–9. https://doi.org/10.1016/j.ijmm.2017.09.016.
25. Bansal-Mutalik R, Nikaido H. Mycobacterial outer membrane is a lipid bilayer and the inner membrane is unusually Rich in Diacyl Phosphatidylinositol Dimannosides. Proc Natl Acad Sci U S A. 2014;111(13):4958–63. https://doi.org/10.1073/pnas.1403078111.
26. Wang L, Slayden RA, Barry CR, Liu J. Cell Wall structure of a mutant of Mycobacterium Smegmatis defective in the biosynthesis of mycolic acids. J Biol Chem. 2000;275(10):7224–9. https://doi.org/10.1074/jbc.275.10.7224.
27. Baek SH, Li AH, Sassetti CM. Metabolic regulation of mycobacterial growth and antibiotic sensitivity. Plos Biol. 2011;9(5):e1001065. https://doi.org/10.1371/journal.pbio.1001065.
28. Hammond RJ, Baron VO, Oravcova K, Lipworth S, Gillespie SH. Phenotypic resistance in Mycobacteria: is it because I am Old or Fat that I resist you? J Antimicrob Chemother. 2015;70(10):2823–7. https://doi.org/10.1093/jac/dkv178.
29. Chuang YM, Bandyopadhyay N, Rifat D, Rubin H, Bader JS, Karakousis PC. Deficiency of the Novel Exopolyphosphatase Rv1026/PPX2 leads to metabolic downshift and altered cell Wall Permeability in Mycobacterium Tuberculosis. Mbio. 2015;6(2):e2428. https://doi.org/10.1128/mBio.02428-14.
30. Zhao F, Yang J, Li J, Li Z, Lin Y, Zheng S, Liang S, Han S. Multiple Cellular responses guarantee yeast survival in Presence of the cell Membrane/Wall Interfering Agent Sodium Dodecyl Sulfate. Biochem Biophys Res Commun. 2020;527(1):276–82. https://doi.org/10.1016/j.bbrc.2020.03.163.
31. Dong W, Wang R, Li P, et al. Orphan Response Regulator Rv3143 increases antibiotic sensitivity by regulating Cell Wall Permeability in Mycobacterium Smegmatis. Arch Biochem Biophys. 2020;692:108522. https://doi.org/10.1016/j.abb.2020.108522.
32. Ghai I, Ghai S. Understanding Antibiotic Resistance Via outer membrane permeability. INFECT DRUG RESIST. 2018;11:523–30. https://doi.org/10.2147/IDR.S156995.
33. Dawan J, Ahn J. Bacterial stress responses as potential targets in overcoming Antibiotic Resistance. Microorganisms. 2022;10(7):1385. https://doi.org/10.3390/microorganisms10071385.
34. Hallgren J, Jonas K. Nutritional Control of bacterial DNA replication. Curr Opin Microbiol. 2024;77:102403. https://doi.org/10.1016/j.mib.2023.102403.
35. Rustad TR, Roberts DM, Liao RP, Sherman DR. Isolation of mycobacterial RNA. Methods Mol Biol. 2009;465:13–21. https://doi.org/10.1007/978-1-59745-207-6_2.
36. Wu Z, Wei W, Zhou Y, Guo H, Zhao J, Liao Q, Chen L, Zhang X, Zhou L. Integrated Quantitative Proteomics and metabolome profiling reveal MSMEG_6171 overexpression perturbing lipid metabolism of Mycobacterium smegmatis leading to increased vancomycin resistance. Front Microbiol. 2020;11:1572. https://doi.org/10.3389/fmicb.2020.01572.
37. Li X, Wu J, Han J, Hu Y, Mi K. Distinct responses of Mycobacterium smegmatis to exposure to Low and high levels of Hydrogen Peroxide. Plos One. 2015;10(7):e134595. https://doi.org/10.1371/journal.pone.0134595.
38. Abdalla AE, Yan S, Zeng J, Deng W, Xie L, Xie J. Mycobacterium tuberculosis Rv0341 promotes Mycobacterium Survival in in Vitro hostile environments and within macrophages and induces cytokines expression. Pathogens. 2020;9(6):454. https://doi.org/10.3390/pathogens9060454.

Publisher's note